Theoretical investigation of charge transfer between N^{6+} and atomic hydrogen

Y. Wu,[1,2,*] P. C. Stancil,[1] H. P. Liebermann,[3] P. Funke,[3] S. N. Rai,[3,†] R. J. Buenker,[3] D. R. Schultz,[4] Y. Hui,[4] I. N. Draganic,[4] and C. C. Havener[4]

[1]*Department of Physics and Astronomy and the Center for Simulational Physics, University of Georgia, Athens, Georgia 30602-2451, USA*

[2]*Institute of Applied Physics and Computational Mathematics, P.O. Box 8009, Beijing 100088, China*

[3]*Fachbereich C–Mathematik und Naturwissenschaften, Bergische Universität Wuppertal, D-42097 Wuppertal, Germany*

[4]*Physics Division, Oak Ridge National Laboratory, Oak Ridge, Tennessee 37831-6372, USA*

(Received 8 April 2011; published 19 August 2011)

Charge transfer due to collisions of ground-state $N^{6+}(1s\,^2S)$ with atomic hydrogen has been investigated theoretically using the quantum-mechanical molecular-orbital close-coupling (QMOCC) method, in which the adiabatic potentials and nonadiabatic couplings were obtained using the multireference single- and double-excitation configuration-interaction (MRDCI) approach. Total, *n*-, *l*-, and *S*-resolved cross sections have been obtained for energies between 10 meV/u and 10 keV/u. The QMOCC results were compared to available experimental and theoretical data as well as to merged-beams measurements and atomic-orbital close-coupling and classical trajectory Monte Carlo calculations. The accuracy of the QMOCC charge-transfer cross sections was found to be sensitive to the accuracy of the adiabatic potentials and couplings. Consequently, we developed a method to optimize the atomic basis sets used in the MRDCI calculations for highly charged ions. Since cross sections, especially those that are state selective, are necessary input for x-ray emission simulation of heliospheric and Martian exospheric spectra arising from solar wind ion–neutral gas collisions, a recommended set of state-selective cross sections, based on our evaluation of the calculations and measurements, is provided.

DOI: 10.1103/PhysRevA.84.022711 PACS number(s): 34.70.+e, 34.20.−b

I. INTRODUCTION

Stemming from use of new space-borne x-ray observatories and the theoretical and experimental work they have motivated, there has been significant progress in x-ray astrophysics over the last decade [1,2], and references therein. For example, the charge-transfer process has been found to play a significant role in the production of the x-rays and extreme ultraviolet (EUV) photons observed from cometary and planetary atmospheres and from the heliosphere [3–5]. This component of the x-ray and EUV emission is due to radiative decay of highly excited ions, formed in the charge-transfer process between heavy solar wind (SW) ions and neutral species in cometary and planetary atmospheres and penetrating the solar system from the local interstellar medium. With the large improvement in photon gathering power of these observatories and the resolution of the detectors that they possess, x-ray observations have been obtained with enhanced spatial and spectral resolution. To explain these spectra, charge-transfer cross sections are required to model the populations of the excited bound states of the ions, which decay radiatively into lower bound states. Despite the significant progress made in both experiment and theory in recent years, the presently available charge-transfer cross sections and rate coefficients are insufficient to meet the needs for x-ray spectral simulations, especially in regard to state-selective cross sections [5].

Charge transfer involving one electron, the single-electron-capture (SEC) process, for N^{6+} colliding with atomic hydrogen is investigated in the present work, because N^{6+} is one of the primary SW minor heavy ions and atomic hydrogen is an abundant neutral species in planetary atmospheres and in the heliosphere. Several groups have reported studies of this collision system. Panov *et al.* [6] measured the total cross section, using a hydrogen-oven gas-cell technique, for a few incident ion energies larger than a few hundred eV/u; likewise Meyer *et al.* [7] measured the total cross section over the energy range 214 eV/u to 7.5 keV/u, and, using a translational energy spectroscopy technique with a RF hydrogen target, Kearns *et al.* [8] measured the energy-change spectrum at 943 eV/u. Panov *et al.* [6] and Kearns *et al.* [8] estimated the charge-transfer cross sections using the Landau-Zener model, while Olson and Salop [9] performed classical trajectory Monte Carlo (CTMC) calculations for a few incident energies larger than 20 keV/u. All these investigations were limited to energies larger than a few hundred eV/u and, to the best our of knowledge, no theoretical results based on an *ab initio* quantum mechanical approach have been reported.

Therefore, in the present work, the quantum-mechanical molecular-orbital close-coupling (QMOCC) method [10,11] has been applied to treat SEC, including total and state-selective cross sections, in which the adopted adiabatic potentials and nonadiabatic couplings were obtained with the multireference single- and double-excitation configuration interaction (MRDCI) approach [12,13]. In order to provide a demonstrably accurate result, we have developed an optimization method for the atomic basis sets used in the MRDCI calculation for highly charged ions. The QMOCC results were compared to available experimental and theoretical data as well as to merged-beams measurements and atomic-orbital close-coupling (AOCC) and CTMC calculations reported here. It should be noted that the collision energy is given in units of eV/u, the center-of-mass energy per reduced mass, which is

*yongwu@physast.uga.edu

†Present address: Department of Physics and Electronics, Bangalore City College, Bangalore 560043, India.

identical to the incident ion energy per ion mass. Otherwise, atomic units (a.u.) are used throughout unless noted.

II. THEORETICAL METHODS

In the present work, the QMOCC, AOCC, and CTMC methods are utilized to calculate total and state-selective cross sections.

A. QMOCC method

1. Electronic structure calculation

In the collision of N^{6+} with atomic hydrogen resulting in SEC, an election is transferred from the hydrogen atom to the nitrogen ion in a state with principal quantum number n most likely equal to 4 or 5. Because the electron originally bound in N^{6+} remains in the tightly bound $1s$ shell, the captured electron's state is essentially hydrogenlike in character. However, the typical basis set adopted in molecular-orbital close-coupling calculations in such cases is the standard set developed for the neutral N atom with the addition of diffuse orbitals. This is clearly an insufficient treatment. Therefore we have developed a hybrid basis set consisting of two components: (i) the standard Dunning neutral N atom basis and (ii) a one-electron basis of hydrogenlike orbitals. The latter basis was optimized to reproduce nearly exactly the hydrogenlike Rydberg ion energies.

Considering N^{5+} as a hydrogenlike ion with effective nuclear charge $Z^* = 6$, a large Gaussian basis set $(17s,11p,9d,6f,3g)$ has been optimized and used for nitrogen. A $(6s,3p,2d,1f)$ basis contracted to $[4s,3p,2d,1f]$ was employed for hydrogen [14]. In the present work, an *ab initio* multireference single- and double-excitation configuration-interaction (CI) calculation [12,13] has been carried out to compute the adiabatic potentials and nonadiabatic coupling matrix elements of the $[NH]^{6+}$ system. Sixteen $^1\Sigma^+$ and fifteen $^3\Sigma^+$ electronic states in A_1 symmetry and ten $^1\Pi$ and ten $^3\Pi$ electronic states in B_1 symmetry have been calculated. Using the optimized Gaussian basis, a full CI calculation was applied for internuclear distances between 1.0 and 50 a.u. Accurate relative asymptotic energies of the $[NH]^{6+}$ system were obtained and compared with the corresponding experimental atomic spectroscopic data [15]. We note that experimental data for some N^{5+} Rydberg levels are lacking. Energies deduced from the calculations of Johnson *et al.* [16] have been utilized in such cases.

As shown in Table I, for the MRDCI calculation with the optimized Gaussian basis set functions, the largest error in the relative asymptotic energies of the $[NH]^{6+}$ system is about 0.05 eV for the important channels with n of 3, 4, and 5, while the error is ∼0.3 eV using the standard Gaussian basis set functions. It should be noted that the resulting ground-state energies of N^{5+} obtained with the standard and the optimized basis sets are −44.775 75 a.u and −44.779 51 a.u, respectively, and the available Hylleraas CI value is −44.788 a.u. In the present MRDCI calculation, the correlation error is greater for the ground state of N^{5+} $(1s^2\,{}^1S)$ than for any of the Rydberg states, which results in underestimations of about 0.33 and 0.23 eV for the ionization energy for the standard and optimized bases, respectively. Given the optimized basis, the nonadiabatic radial and rotational coupling elements are calculated by applying a finite-difference method [12] with the wave functions obtained.

2. QMOCC scattering method

The QMOCC method has been described thoroughly in previous work [10,11]. In brief, it involves solution of a coupled set of second-order differential equations using the log-derivative method of Johnson [17]. In the adiabatic representation, transitions between channels are driven by radial and rotational ($A^{\rm rad}$ and $A^{\rm rot}$) couplings of the vector potential $\vec{A}(\vec{R})$, where $\vec{R}$ is the internuclear distance vector. Since the adiabatic description contains first- and second-order derivatives, it is numerically convenient to make a unitary transformation [10,18–20] to a diabatic representation,

$$U(R) = W(R)[V(R) - P(R)]W^{-1}(R) \tag{1}$$

and

$$dW(R)/dR + W(R)A^{\rm rad}(R) = 0, \tag{2}$$

where $U(R)$ is the diabatic potential matrix, $V(R)$ the diagonal adiabatic potential, $W(R)$ a unitary transformation matrix, and $P(R)$ the rotational coupling matrix whose elements are given by [11,21,22]

$$P_{\alpha\beta} = \mp\frac{1}{\mu R^2}(J \mp \Lambda_\alpha)(J \pm \Lambda_\alpha + 1)^{1/2} A^{\rm rot}_{\alpha\beta}\delta(\Lambda_\alpha, \Lambda_\beta \mp 1). \tag{3}$$

With the diabatic potentials and couplings, the coupled set of second-order differential equations is solved and matched to the plane-wave boundary conditions at large internuclear separation ($R = 200$) to obtain the K matrix, and from it the S matrix [10]. The total charge-transfer cross section is then given by

$$\sigma_{\alpha\to\beta} = \frac{\pi g_\alpha}{k^2}\sum(2J+1)|(S_J)_{\alpha\beta}|^2, \tag{4}$$

where the unitary S matrix for each partial wave J is defined as

$$S_J = [I + iK_J]^{-1}[I - iK_J]. \tag{5}$$

I is the identity matrix, k denotes the wave number for center-of-mass motion of the initial ion-atom channel, and g_α is an approach probability factor of the initial channel α. The procedure described above is carried out with increasing number of partial waves until the cross section converges.

B. AOCC method

Complementary to the close-coupling approach used at low collision energies utilizing molecular-orbital wave functions, methods based on use of atomic orbitals are more appropriate at higher collision energies. Thus, the most widely used quantum mechanical method to treat charge transfer for intermediate energies, say above ∼1 keV/u, is the atomic-orbital close-coupling approach (see the review by Fritsch and Lin [23] or standard texts [21,24]). In this method, the time-dependent electronic wave function is expanded in terms of functions such as those of the atomic orbitals of the isolated target and projectile or other functions such as Gaussians or

TABLE I. Comparison between the experimental data [15] and the MRDCI calculation for the relative asymptotic energies (eV) of the $[NH]^{6+}$ system. The energies E_1 and E_2 have been obtained with the standard and the optimized Gaussian basis set functions, respectively, and ΔE_1 and ΔE_2 are the corresponding energy differences between the calculations and measurements E_0, $\Delta E_1 = E_0 - E_1$ and $\Delta E_2 = E_0 - E_2$. Different energy zero points are adopted for $\Delta E_1^{(1)}$ and $\Delta E_1^{(2)}$ and for $\Delta E_2^{(1)}$ and $\Delta E_2^{(2)}$, respectively.

Molecular states	E_0	E_1	$\Delta E_1^{(1)}$	$\Delta E_1^{(2)}$	E_2	$\Delta E_2^{(1)}$	$\Delta E_2^{(2)}$
$1\,^1\Sigma^+[N^{5+}(1s\,1s\,^1S) + H^+]$	0.0	0.0	0.0	−0.31427	0.0	0.0	−0.24121
$2\,^1\Sigma^+[N^{5+}(1s2s\,^1S) + H^+]$	426.4156	426.21543	0.20017	−0.1141	426.25487	0.16073	−0.08048
$3\,^1\Sigma^+[N^{5+}(1s2p\,^1P_o) + H^+]$	430.695	430.5757	0.11930	−0.19497	430.52569	0.16931	−0.0719
$4\,^1\Sigma^+[N^{5+}(1s3s\,^1S) + H^+]$	496.6807	496.47947	0.20123	−0.11304	496.47792	0.20278	−0.03843
$5\,^1\Sigma^+[N^{5+}(1s3d\,^1D) + H^+]$	497.644	497.52263	0.12137	−0.1929	497.44499	0.19901	−0.0422
$6\,^1\Sigma^+[N^{5+}(1s3p\,^1P_o) + H^+]$	497.9689	497.697	0.27190	−0.04237	497.71457	0.25433	0.01312
$7\,^1\Sigma^+[N^{5+}(1s4s\,^1S) + H^+]$	521.046	520.81873	0.22727	−0.087	520.83193	0.21407	−0.02714
$8\,^1\Sigma^+[N^{5+}(1s4d\,^1D) + H^+]$	521.4564	521.37329	0.08311	−0.23116	521.23714	0.21926	−0.02195
$9\,^1\Sigma^+[N^{5+}(1s4f\,^1F_o) + H^+]$	521.4680[a]	521.46704	0.00104	−0.31323	521.24417	0.22391	−0.0173
$10\,^1\Sigma^+[N^{5+}(1s4p\,^1P_o) + H^+]$	521.5779	521.57481	0.00309	−0.31118	521.36889	0.20901	−0.0322
$11\,^1\Sigma^+[N^{5+}(1s5s\,^1S) + H^+]$	532.2666	532.02214	0.24446	−0.06981	532.05180	0.21480	−0.02641
$12\,^1\Sigma^+[N^{5+}(1s5d\,^1D) + H^+]$	532.4712	532.45702	0.01418	−0.30009	532.24854	0.22266	−0.01855
$13\,^1\Sigma^+[N^{5+}(1s5g\,^1G) + H^+]$	532.5112[a]	532.48966	0.02154	−0.29273	532.26028	0.25092	0.00971
$14\,^1\Sigma^+[N^{5+}(1s5f\,^1F_o) + H^+]$	532.5212[a]	532.49952	0.02168	−0.29259	532.26616	0.25504	0.01383
$15\,^1\Sigma^+[N^{5+}(1s5p\,^1P_o) + H^+]$	532.6472	532.60899	0.03821	−0.27606	532.41312	0.23408	−0.00713
$16\,^1\Sigma^+[N^{6+}(1s\,^2S) + H(1s\,^2S)]$	537.1110[b]	536.79676	0.31427	0	536.86982	0.24121	0
$1\,^3\Sigma^+[N^{5+}(1s2s\,^3S) + H^+]$	419.7968	419.60043	0.196370	−0.11502	419.65092	0.14588	−0.09826
$2\,^3\Sigma^+[N^{5+}(1s2p\,^3P_o) + H^+]$	426.31708	426.2105	0.106578	−0.20481	426.10611	0.21097	−0.03317
$3\,^3\Sigma^+[N^{5+}(1s3s\,^3S) + H^+]$	494.9275	494.72267	0.204834	−0.10656	494.72717	0.20033	−0.04381
$4\,^3\Sigma^+[N^{5+}(1s3p\,^3P_o) + H^+]$	496.7005	496.46584	0.234662	−0.07673	496.47439	0.22611	−0.01803
$5\,^3\Sigma^+[N^{5+}(1s3d\,^3D) + H^+]$	497.6056	497.48927	0.116326	−0.19506	497.40215	0.20345	−0.04069
$6\,^3\Sigma^+[N^{5+}(1s4s\,^3S) + H^+]$	520.3369	520.11585	0.221049	−0.09034	520.11703	0.21987	−0.02427
$7\,^3\Sigma^+[N^{5+}(1s4p\,^3P_o) + H^+]$	521.0584	521.06884	−0.0104389	−0.32183	520.84599	0.21241	−0.03173
$8\,^3\Sigma^+[N^{5+}(1s4d\,^3D) + H^+]$	521.4552	521.35751	0.0976865	−0.2137	521.21662	0.23858	−0.00556
$9\,^3\Sigma^+[N^{5+}(1s4f\,^3F_o) + H^+]$		521.4697			521.23721		
$10\,^3\Sigma^+[N^{5+}(1s5s\,^3S) + H^+]$	531.9108	531.67786	0.232938	−0.07845	531.73	0.1808	−0.06334
$11\,^3\Sigma^+[N^{5+}(1s5p\,^3P_o) + H^+]$	532.274	532.2671	0.00690110	−0.30449	532.18734	0.08666	−0.15748
$12\,^3\Sigma^+[N^{5+}(1s5d\,^3D) + H^+]$	532.4588	532.45084	0.00796065	−0.30343	532.242	0.2168	−0.02734
$13\,^3\Sigma^+[N^{5+}(1s5f\,^3F_o) + H^+]$		532.49242			532.25266		
$14\,^3\Sigma^+[N^{5+}(1s5g\,^3G) + H^+]$		532.4953			532.25735		
$15\,^3\Sigma^+[N^{6+}(1s\,^2S) + H(1s\,^2S)]$	537.11103[b]	536.79964	0.311390	0	536.86689	0.24414	0

[a]From the calculations of Johnson *et al.* [16].

[b]The Coulomb repulsion $5/R$ has been subtracted at $R = 100$ a.u between N^{5+} and H^+.

Sturmians that may span not only the bound states but also the continuum. As in several other recent works [27–31], for comparison with other methods, here the present QMOCC results, we utilize the AOCC with pseudostates method of Kuang and Lin [25,26], a so-called semiclassical approach using a straight-line trajectory for the projectile's motion owing to the validity of this approximation for intermediate and high collision velocities.

The present AOCC approach considers the collision system as possessing one active electron, so we adopted a model potential [32] to represent the interaction of this electron with the N^{6+} ion. Eigensolution with the basis functions of the Kuang and Lin method was performed to obtain the basis set. For each collision energy, solution of the coupled equations was then performed and the probabilities for transitions to these states were computed as a function of impact parameter, yielding the cross sections for charge transfer to individual states within the basis set. For the higher collision energies considered here, up to 195 basis states were used (up to 86 on the atomic hydrogen atom from the $1s$ level to $11f$, and up to 109 on the N^{5+} product ion from $2s$ to $10g$, with many of the highest states in the pseudocontinuum). For the lowest collision energies, the basis had to be reduced for numerical stability, containing as few as 89 states (10 on the hydrogen atom, $1s$–$3d$, and 79 on the nitrogen ion, $2s$–$8g$).

C. CTMC method

Also useful for comparison with the QMOCC results are those obtained from application of the CTMC method, particularly for intermediate collision energies and charge transfer to higher principal quantum numbers. This method simulates an ion-atom collision by sampling trajectories stemming from initial electronic orbits within a large ensemble of configurations [33,34] (see also recent work using CTMC to compute state-selective charge transfer, such as Refs. [28,30,31]). The initial electronic orbitals are prepared in such a way as to mimic the quantum mechanical electronic

momentum distribution. The motion of the particles is then determined by an iterative solution of Hamilton's equations using either Coulomb (for the electron-proton interaction in H) or model (for the electron-N^{6+} and proton-N^{6+} interactions) potentials. At an asymptotic distance, the relative classical binding energies are then calculated to determine if a reaction (charge transfer, excitation, or ionization) has occurred. Following binning rules [35], modified to account for the structure of the N^{6+} ion [36], the final quantum state after charge transfer can then be determined based on the binding energy and angular momentum of the electron if it is bound to the projectile ion.

III. RESULTS AND DISCUSSION

For the energy range 0.01–10^4 eV/u, the exoergic channels are the most important for charge transfer and, therefore, 22 channels were included in the QMOCC calculations for both the singlet and triplet manifolds. They included 4 $^1\Sigma^+$–16 $^1\Sigma^+$, 3 $^3\Sigma^+$–15 $^3\Sigma^+$, 2 $^1\Pi$–10 $^1\Pi$, and 2 $^3\Pi$–10 $^3\Pi$. As can be seen in Table I, the energy gap between the 3 $^1\Sigma^+$ and 4 $^1\Sigma^+$ states is larger than 65 eV in the asymptotic region, and there are similar energy gaps between the 1 $^1\Pi$ and 2 $^1\Pi$, 2 $^3\Sigma^+$ and 3 $^3\Sigma^+$, and 1 $^3\Pi$ and 2 $^3\Pi$ states. Consequently, charge transfer to these states is not expected to be significant for the range of collision energies considered using the QMOCC method. For higher collision energies, the AOCC and CTMC methods have been used to obtain the total and state-selective (*nl*-dependent) cross sections including endoergic channels.

A. Potentials and couplings

As a consequence of the initial channel symmetries ($^1\Sigma^+$ and $^3\Sigma^+$) and the fact that rotational coupling is considered, the $^1\Pi$ and $^3\Pi$ channels are also involved in the QMOCC charge-transfer calculations. In Fig. 1, the adiabatic potential curves are presented for these important channels, including

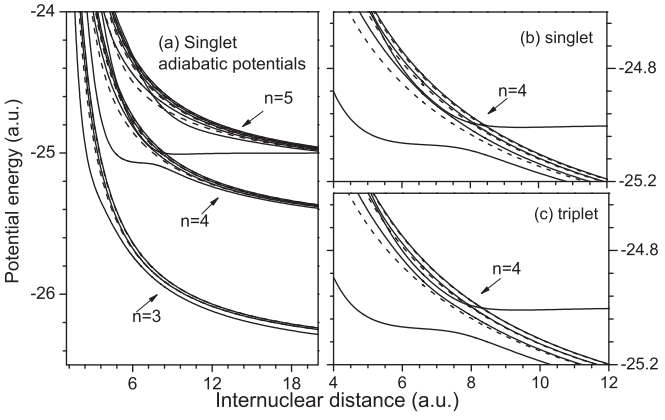

FIG. 1. Adiabatic potentials for $[NH]^{6+}$ states as a function of internuclear distance. (a) Adiabatic potentials for singlet states; (b),(c) adiabatic potentials for the most important $n = 4$ channels close to the avoided crossings at $R = 8$ a.u. for both singlet (b) and triplet (c) states. Note that the curves in (a) are 4 $^1\Sigma^+$, 5 $^1\Sigma^+$, 2 $^1\Pi$, 6 $^1\Sigma^+$, 3 $^1\Pi$, 7 $^1\Sigma^+$, 8 $^1\Sigma^+$, 4 $^1\Pi$, 5 $^1\Pi$, 9 $^1\Sigma^+$, 6 $^1\Pi$, 10 $^1\Sigma^+$, 11 $^1\Sigma^+$, 12 $^1\Sigma^+$, 7 $^1\Pi$, 13 $^1\Sigma^+$, 8 $^1\Pi$, 14 $^1\Sigma^+$, 9 $^1\Pi$, 15 $^1\Sigma^+$, 10 $^1\Pi$, and 16 $^1\Sigma^+$ from bottom to top at $R = 50$ a.u.

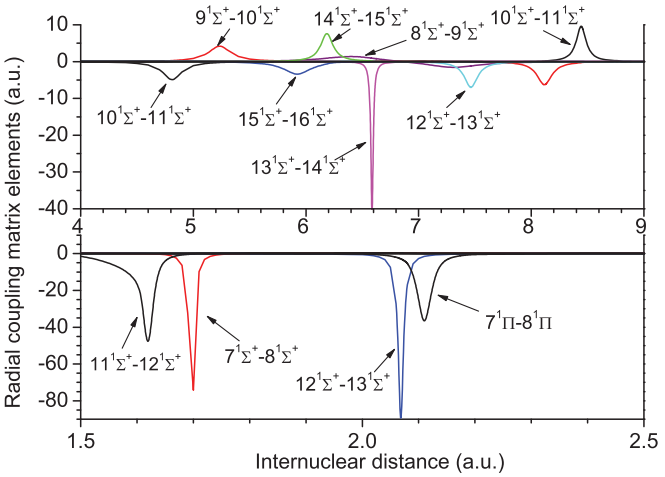

FIG. 2. (Color online) Nonadiabatic radial couplings for the adjacent channels of the singlet states of $[NH]^{6+}$ (both $^1\Sigma^+$ and $^1\Pi$) as a function of internuclear distance.

both singlet and triplet spin symmetries. Since there are many channels considered in the present calculation, only the radial and rotational couplings for the adjacent channels for the singlet states are presented as an illustration, shown in Figs. 2 and 3, respectively. In Table II, the avoided-crossing distances R_x for the adiabatic states of the system are presented and compared with estimates made using the experimental asymptotic energies, which can provide an effective check of the calculation for avoided crossings at large internuclear distances. We note that, compared with the calculation of $R_x^{(1)}$, made using the standard Gaussian basis set, there is better agreement with the experimental value ($R_x^{(0)}$) with $R_x^{(2)}$, made using the optimized Gaussian basis set.

B. Cross sections

Using the adiabatic potentials and nonadiabatic coupling matrix elements obtained with the MRDCI approach, the

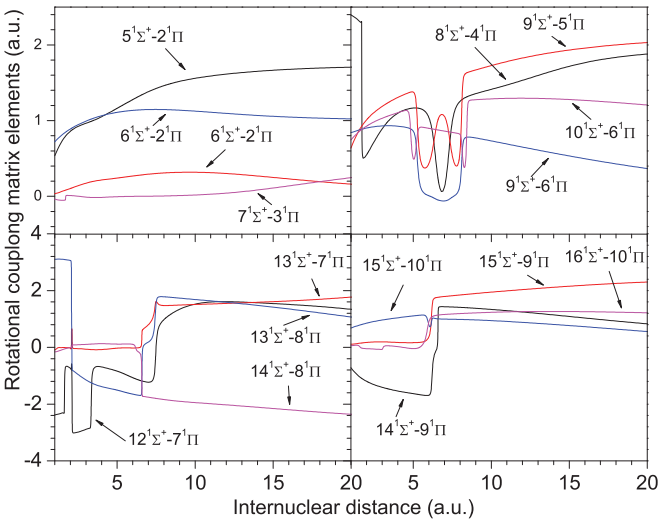

FIG. 3. (Color online) Nonadiabatic rotational couplings for the adjacent $^1\Sigma^+$ and $^1\Pi$ channels of $[NH]^{6+}$ as a function of internuclear distance.

TABLE II. Comparison between the avoided-crossing distances (R_x) for the adiabatic states of $[NH]^{6+}$ from the experimental data [15] and from the MRDCI calculation. $R_x^{(0)}$ is the value estimated from experimental data, and $R_x^{(1)}$ and $R_x^{(2)}$ are obtained from the MRDCI calculation with the standard and the optimized Gaussian basis set functions, respectively.

Atomic states	$R_x^{(0)}$(a.u)	$R_x^{(1)}$(a.u)	$R_x^{(2)}$(a.u)	Atomic states	$R_x^{(0)}$(a.u)	$R_x^{(1)}$(a.u)	$R_x^{(2)}$(a.u)
$N^{5+}(1s4s\ ^1S) + H^+$	7.81	7.5	7.26	$N^{5+}(1s4s\ ^3S) + H^+$	7.50	7.65	7.50
$N^{5+}(1s4d\ ^1D) + H^+$	8.00	7.55	7.31	$N^{5+}(1s4p\ ^3P^o) + H^+$	7.81	7.70	7.56
$N^{5+}(1s4f\ ^1F^o) + H^+$	8.00	8.24	8.12	$N^{5+}(1s4d\ ^3D) + H^+$	8.00	8.07	7.93
$N^{5+}(1s4p\ ^1P^o) + H^+$	8.05	8.55	8.44	$N^{5+}(1s4f\ ^3F^o) + H^+$		8.43	8.31
$N^{5+}(1s5s\ ^1S) + H^+$	21.93	22.0	21.3	$N^{5+}(1s5s\ ^3S) + H^+$	20.74	20.7	21.3
$N^{5+}(1s5d\ ^1D) + H^+$	22.67	23.1	22.3	$N^{5+}(1s5p\ ^3P^o) + H^+$	21.95	22.7	22.1
$N^{5+}(1s5g\ ^1G) + H^+$	22.83	23.9	22.8	$N^{5+}(1s5d\ ^3D) + H^+$	22.63	23.5	22.8
$N^{5+}(1s5f\ ^1F^o) + H^+$	22.87	24.4	23.3	$N^{5+}(1s5f\ ^3F^o) + H^+$		24.4	23.3
$N^{5+}(1s5p\ ^1P^o) + H^+$	23.36	24.9	23.8	$N^{5+}(1s5g\ ^3G) + H^+$		24.9	23.8

QMOCC method was used to calculate the total and state-selective SEC cross sections for collisions of N^{6+} with atomic hydrogen in the energy range of 10 meV/u to 10 keV/u. The total cross sections are displayed in Fig. 4 along with available experimental and theoretical data. For energies between ~500 and 3000 eV/u, which covers the kinetic energy range of SW ions, there is good agreement between the present QMOCC and AOCC calculations and fair agreement with the measurements of Meyer *et al.* [37] and merged-beams measurements [38]. For the highest energies considered in the QMOCC calculation (>7 keV/u), the total cross section is found to be overestimated, which may be due to a limited N^{5+} basis, the neglect of the ionization channel, and/or the neglect of electron translation factors.

For collision energies less than about 500 eV/u, a significant discrepancy is evident between the QMOCC total cross sections and the merged-beams measurements. This difference is troublesome as the AOCC results are consistent with the measurements down to 100 eV/u. However, three facts give some confidence in the low-energy QMOCC results. First, similar differences have been noted between measurements, using other experimental techniques, and QMOCC findings for highly charged ions colliding with atomic hydrogen. These include fully stripped and H-like C, N, O, F, and Ne from relatively low energies up to a few hundred or a few thousand eV/u [7,37,39]. For fully stripped ions, this is somewhat surprising since the quantal treatment of a one-electron system is thought to be reliable. Second, for systems involving low-charged ions, good agreement has been found at low energies, down to a few eV/u, for $C^{3+} + H$ [40], $O^{3+} + H$ [11], $N^{4+} + H$ [41], and $H^+ + H$ [42], for example. Third, straight-line trajectories were adopted in the current AOCC approach, which is expected to be less reliable at the lower energies. We also note that oscillatory structures are predicted by the QMOCC method at very low energies (<0.1 eV/u); such structures have been found in other systems [43]. As a consequence, the origin of the low-energy discrepancy is unknown, but a number of factors may contribute. For example, for highly charged ion systems, postcollisional interactions via strong Coulomb repulsion between the product protons (after charge exchange) and residual incident N^{6+} beam ions and product N^{5+} may deflect the protons into large scattering angles, while remaining uncertainties in the QMOCC computations may result from uncertainties in the potential energies (particularly near avoided crossings), nonadiabatic couplings, and coupling phases.

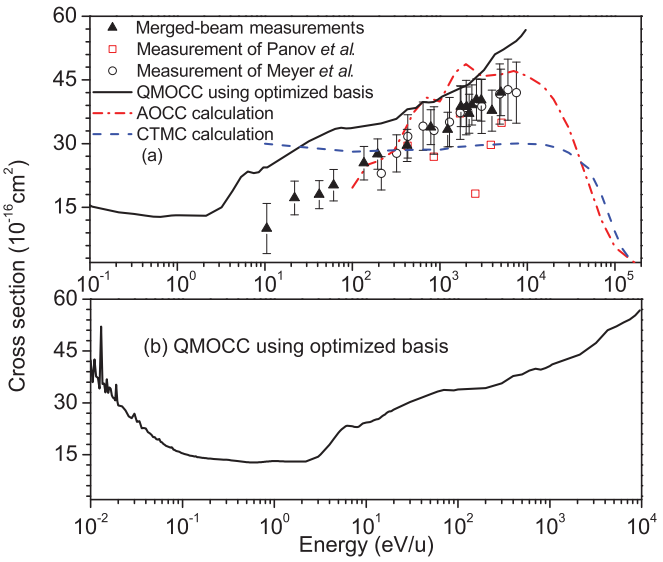

FIG. 4. (Color online) Total SEC cross section for $N^{6+} + H$ collisions. Black line, the present QMOCC calculation obtained with the optimized Gaussian basis set; red dot-dashed line, the present AOCC calculation; blue dashed line, the present CTMC calculation; filled triangles, merged-beams measurements [38]; filled circles with error bars, measurements of Meyer *et al.* [7]; filled squares, measurements of Panov *et al.* [6].

In Fig. 5, the present QMOCC calculations of state-selective charge-transfer cross section are presented. The contributions from the $n = 4$ channels are dominant over the whole energy range, but contributions from the $n = 5$ and $n = 3$ channels increase rapidly with increasing energy. At an energy of about 5000 eV/u, the contributions from the $n = 5$ channels equal that of the $n = 4$ channels, because of avoided-crossing interactions at very small R. However, because the $n = 5$ channels are the highest of those included in the QMOCC scattering calculation, the corresponding cross sections are likely to be overestimated, particularly those for the $5p\ ^1P$ and $5g\ ^3G$ channels. With a further increase in energy, contributions from the $n = 2$ and 3 and $n > 5$ channels, not included in the QMOCC calculations, become important as discussed below.

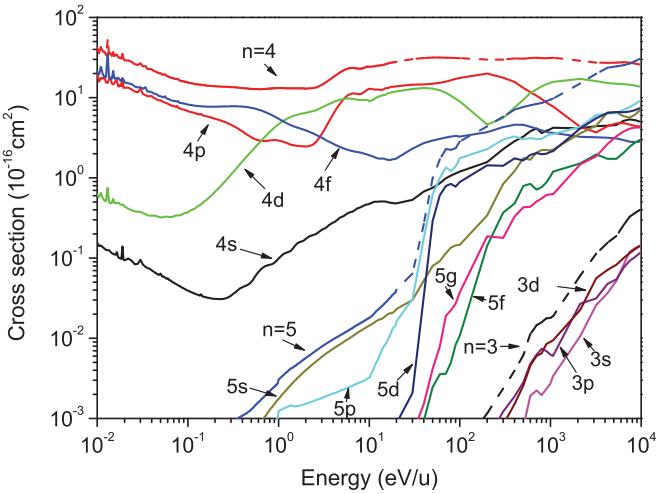

FIG. 5. (Color online) QMOCC calculations of state-selective charge-transfer cross section in N^{6+} + H collisions.

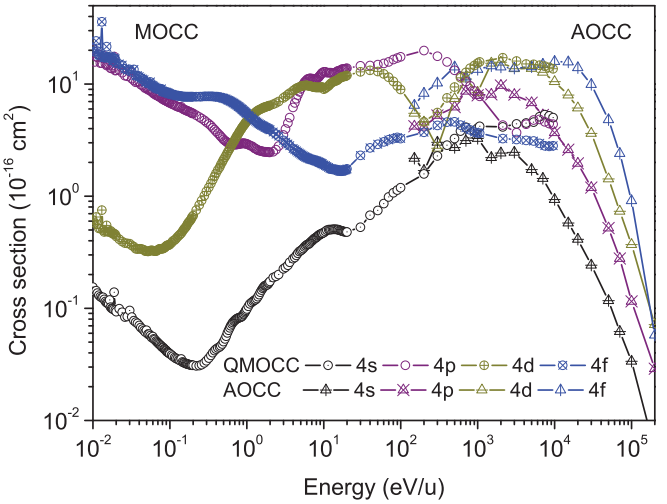

FIG. 7. (Color online) The l-resolved SEC cross sections obtained with the QMOCC and AOCC methods for the $n = 4$ channels.

In Fig. 6, the n-resolved cross sections obtained using the QMOCC, AOCC, and CTMC methods are compared for $n = 2$–9. All the calculations consistently find that the $n = 4$ channels dominate. The $n = 5$ channels are also important, with cross sections much larger than those of $n = 3$ for the QMOCC and AOCC calculations (the $n = 3$ contribution is found to dominate over $n = 5$ in the less applicable, low-energy, low-n-level CTMC calculation). In Fig. 7, the $n = 4$,l cross sections from the QMOCC and AOCC methods are compared. Near 1 keV/u, the two methods give very similar results for all channels, except the $4f$. This is likely due to the fact that the QMOCC calculations account for the spin dependence of the cross sections and the irregular internal energy ordering of the $4l$ singlet states (see Table I). The behavior of the CTMC calculation (not shown for simplicity) is again somewhat different, with the two dominant channels being the $4s$ and $4f$.

The l distributions of the QMOCC results at 1 keV/u and 300 eV/u for the $n = 4$ channels are presented and compared with those from the AOCC and CTMC calculations, a statistical distribution, and the "low-energy distribution" proposed by Janev *et al.* [44] and Abramov *et al.* [45] in Fig. 8. The latter is proposed to be appropriate for typical SW ion energies, while the statistical distribution is applicable

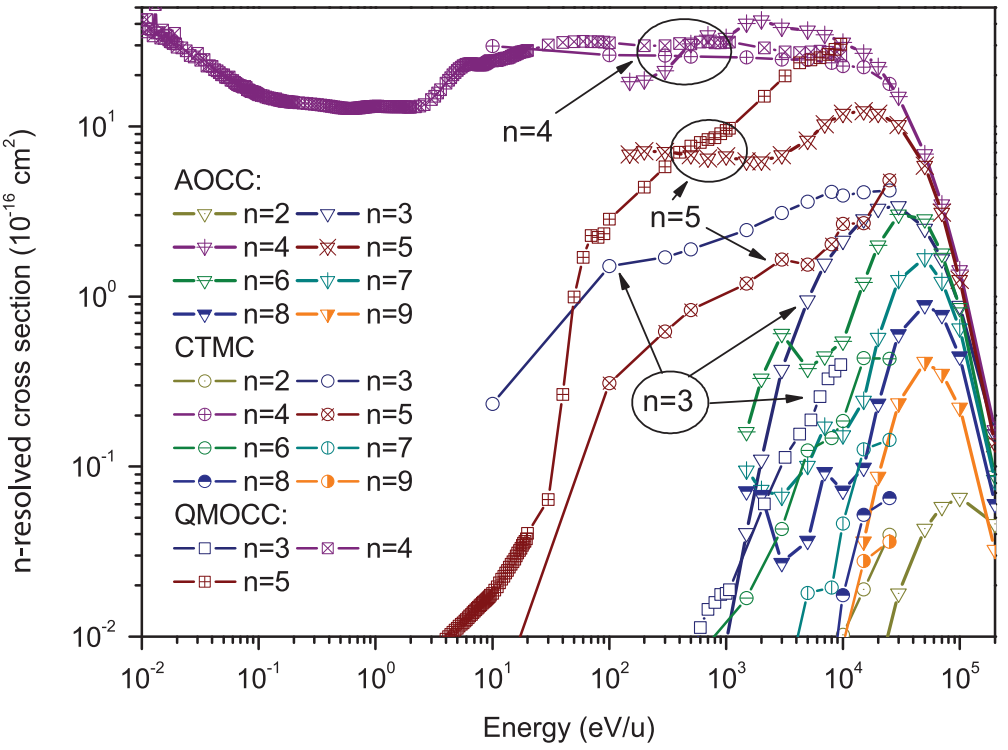

FIG. 6. (Color online) The N^{6+} + H n-resolved SEC cross sections using the MOCC, AOCC, and CTMC methods.

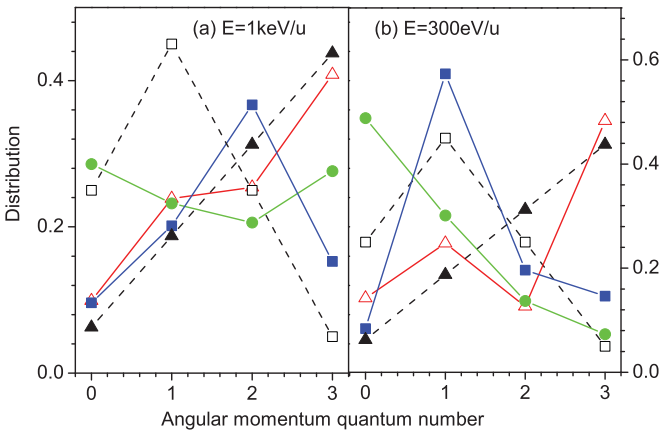

FIG. 8. (Color online) $N^{6+} + H \rightarrow N^{5+} + H^{+}$ l distribution after SEC at 1 keV/u and 300 eV/u ($n = 4$). Solid line with filled squares, QMOCC; solid line with unfilled triangles, AOCC; solid line with filled circles, CTMC; dashed line with unfilled squares, low-energy distribution [44,45]; dashed line with filled triangles, statistical distribution.

for higher energies ($E \gg 10$ keV/u). The present QMOCC l distribution is most similar to the low-energy distribution at 1 keV/u, while they are nearly identical at 300 eV/u. The AOCC results are most similar to a statistical distribution, while the CTMC distributions are intermediate between the two cases. The current results suggest that neither analytical distribution function nor the CTMC method are sufficiently reliable to predict final nl populations for collision energies typical of SW ions, as independently observed by Ali *et al.* [46]. However, the low-energy and statistical distributions may be useful for approximating conditions at slow and fast solar wind speeds, respectively, in the absence of more applicable, explicit calculations (see [30]).

In Fig. 9, the QMOCC cross-section ratios for charge transfer to the total triplet and singlet states are presented and

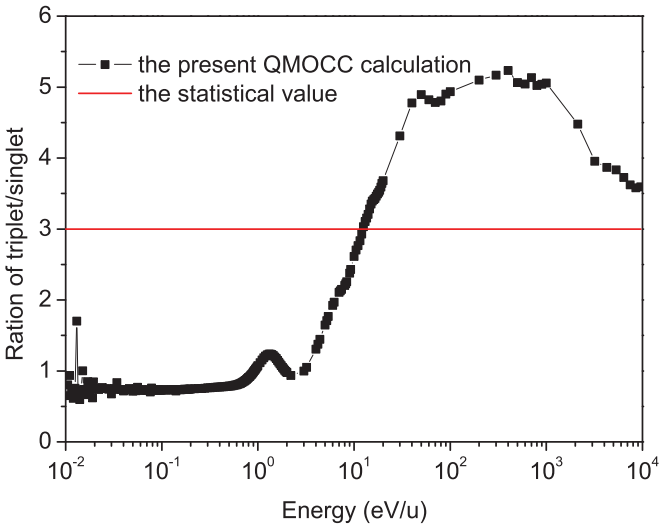

FIG. 9. (Color online) Cross-section ratios for SEC to the triplet and singlet states. Solid line with filled squares, the present QMOCC results obtained with the optimized Gaussian basis set; red line, the statistical value of 3.

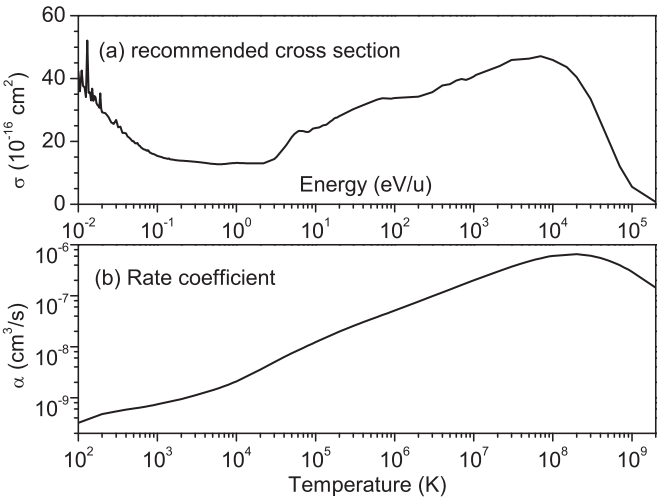

FIG. 10. Recommended total cross section and the corresponding total rate coefficients for SEC in collisions of N^{6+} with H.

compared to the statistical value of 3. The QMOCC results only start to converge to the statistical value as the collision energy increases to a few keV/u, with the ratio reaching about 3.5 at 10 keV/u. At higher energy, the actual ratio can be expected to approach the statistical limit. For typical solar wind speeds, the ratio is about 5. The present calculations reveal that singlet and triplet initial states contribute differently to capture processes, and there are strong influences of the electron-electron interaction during the collision. Due to varying electron correlation effects in the singlet and triplet states, the excitation energy intervals are different and the energy orderings modified for some singlet states (see Table I). Thus, the present calculation indicates the degree to which the assumption of a 3:1 ratio of triplet to singlet cross sections would be valid for this case, and raises the possibility that this common approximation for other collision systems should be questioned [3]. Further, the variation in the triplet-singlet ratio for nl-resolved cross sections (not shown) can be even larger.

In order to apply the present results conveniently in models of x-ray emission and other applications, a recommended set of total and state-selective cross sections has been constructed over a large energy range based on the present QMOCC, AOCC, and CTMC results. The QMOCC results are utilized for energies less than 3 keV/u, while for higher energies the AOCC calculations were adopted with the CTMC results used in some cases. To approximate spin resolution in the AOCC- and CTMC-based cross sections, they were scaled by the QMOCC triplet-to-singlet ratio at 3 keV/u and smoothly varied to a ratio of 3 at higher energies. The recommended total cross section is displayed in Fig. 10(a) while the state-selective cross sections can be obtained upon request. Using the recommended cross sections, the total rate coefficient has also been computed, as displayed in Fig. 10(b).

IV. CONCLUSIONS

In the present work, single-electron capture due to collisions of $N^{6+}(1s\,^2S)$ with atomic hydrogen has been investigated using the QMOCC, AOCC, and CTMC methods. We

developed a hybrid basis set for the MRDCI calculation for highly charged ions and accurate adiabatic potentials, and nonadiabatic radial and rotational couplings were obtained. For the kinetic energy of solar wind ions, $E \sim 500$–$5000\,\mathrm{eV/u}$, there is good agreement between the AOCC, QMOCC, and experimental results for the total cross section. n-, l-, and S-resolved SEC state-selective cross sections were also obtained, and will be of importance for accurate predictions of x-ray emission following charge transfer arising from solar wind ion interactions with cometary and planetary atmospheres and heliospheric neutral species.

ACKNOWLEDGMENTS

This work was partially supported by NASA Grant Nos. NNX09AV46G, NNG09WF24I, and NNH07ZDA001N.

[1] T. R. Kallman and P. Palmeri, Rev. Mod. Phys. **79**, 79 (2007).
[2] A. Bhardwaj *et al.*, Planet. Space Sci. **55**, 1135 (2007).
[3] V. A. Krasnopolsky, J. B. Greenwood, and P. C. Stancil, Space Sci. Rev. **113**, 271 (2004).
[4] R. Ali, P. A. Neill, P. Beiersdorfer, C. L. Harris, M. J. Raković, J. G. Wang, D. R. Schultz, and P. C. Stancil, Astrophys. J. Lett. **629**, L125 (2005).
[5] P. C. Stancil, J. G. Wang, M. J. Raković, D. R. Schultz, and R. Ali, in *Atomic and Molecular Data and Their Applications*, edited by D. R. Schultz, P. S. Krstić, and F. Ownby, AIP Conf. Proc. No. 636 (AIP, New York, 2002), p. 144.
[6] M. N. Panov, A. A. Basalaev, and K. O. Lozhkin, Phys. Scr., T **3**, 124 (1983).
[7] F. W. Meyer, A. M. Howald, C. C. Havener, and R. A. Phaneuf, Phys. Rev. A **32**, 3310 (1985).
[8] D. M. Kearns, R. W. McCullough, R. Trassl, and H. B. Gilbody, J. Phys. B **36**, 3653 (2003).
[9] R. E. Olson and A. Salop, Phys. Rev. A **16**, 531 (1977).
[10] B. Zygelman, D. L. Cooper, M. J. Ford, A. Dalgarno, J. Gerratt, and M. Raimondi, Phys. Rev. A **46**, 3846 (1992).
[11] J. G. Wang, P. C. Stancil, A. R. Turner, and D. L. Cooper, Phys. Rev. A **67**, 012710 (2003).
[12] R. J. Buenker, and S. D. Peyerimhoff, Theor. Chim. Acta **35**, 33 (1974); **39**, 217 (1975); R. J. Buenker, Int. J. Quantum Chem. **29**, 435 (1986); in *Proceedings of the Workshop on Quantum Chemistry and Molecular Physics*, edited by P. G. Burton (University of Wollongong Press, Wollongong, Australia, 1980), p. 1.5.1.; *Current Aspects of Quantum Chemistry 1981*, edited by R. Carbo, Studies in Physical and Theoretical Chemistry Vol. 21 (Elsevier, Amsterdam, 1982), pp. 17 and 81.
[13] R. J. Buenker and R. A. Phillips, J. Mol. Struct. (THEOCHEM) **123**, 291 (1985); S. Krebs and R. J. Buenker, J. Chem. Phys. **103**, 5613 (1995); R. J. Buenker and S. Krebs, in *Recent Advances in Multireference Methods*, edited by K. Hirao (World Scientific, Singapore, 1999), p. 1.
[14] T. H. Dunning Jr., J. Chem. Phys. **90**, 1007 (1989).
[15] R. L. Kelly, J. Phys. Chem. Ref. Data Suppl. **16**, 1 (1987).
[16] W. R. Johnson, I. M. Savukov, U. I. Safronova, and A. Dalgarno, Astrophys. J. Suppl. **141**, 543 (2002).
[17] B. R. Johnson, J. Comput. Phys. **13**, 445 (1973).
[18] T. G. Heil, S. E. Butler, and A. Dalgarno, Phys. Rev. A **27**, 2365 (1983).
[19] D. L. Cooper, N. J. Clarke, P. C. Stancil, and B. Zygelman, Adv. Quantum Chem. **40**, 37 (2001).
[20] F. T. Smith, Phys. Rev. **179**, 111 (1969).
[21] B. H. Bransden and M. R. C. McDowell, *Charge Exchange and the Theory of Ion-Atom Collisions* (Clarendon Press, Oxford, 1992).
[22] A. R. Turner, D. L. Cooper, J. G. Wang, and P. C. Stancil, Phys. Rev. A **68**, 012704 (2003).
[23] W. Fritsch and C. D. Lin, Phys. Rep. **202**, 1 (1991).
[24] M. R. C. McDowell and J. P. Coleman, *An Introduction to the Theory of Ion-Atom Collisions* (North-Holland, Amsterdam, 1970).
[25] J. Kuang and C. D. Lin, J. Phys. B **29**, 1207 (1996).
[26] J. Kuang and C. D. Lin, J. Phys. B **29**, 5443 (1996).
[27] M. S. Pindzola, T-G. Lee, T. Minami, and D. R. Schultz, Phys. Rev. A **72**, 062703 (2005).
[28] T. Minami, M. S. Pindzola, T-G. Lee, and D. R. Schultz, J. Phys. B **39**, 2877 (2006).
[29] T. Minami, M. S. Pindzola, T-G. Lee, and D. R. Schultz, J. Phys. B **40**, 3629 (2007).
[30] T. Minami, T. G. Lee, M. S. Pindzola, and D. R. Schultz, J. Phys. B **41**, 135201 (2008).
[31] D. R. Schultz, T. G. Lee, and S. D. Loch, J. Phys. B **43**, 144002 (2010).
[32] E. Edgu Fry, A. Wech, J. Stuhlman, T. G. Lee, C. D. Lin, and C. L. Cocke, Phys. Rev. A **69**, 052714 (2004).
[33] R. Abrines and I. C. Percival, Proc. Phys. Soc. London **88**, 861 (1966).
[34] R. E. Olson and A. Salop, Phys. Rev. A **16**, 531 (1977).
[35] R. L. Becker and A. D. MacKellar, J. Phys. B **17**, 3923 (1984).
[36] D. R. Schultz, P. C. Stancil, and M. J. Raković, J. Phys. B **34**, 2739 (2001).
[37] F. W. Meyer, Nucl. Instrum. Methods Phys. Res., Sect. B **9**, 532 (1985).
[38] C. C. Havener, I. N. Draganic, D. R. Schultz, Y. Wu, and P. C. Stancil (unpublished).
[39] R. A. Phaneuf, I. Alvarez, F. W. Meyer, and D. H. Crandall, Phys. Rev. A **26**, 1892 (1982).
[40] C. C. Havener, A. Muller, P. A. Zeijlmans van Emmichoven, and R. A. Phaneuf, Phys. Rev. A **51**, 2982 (1995).
[41] L. Folkerts, M. A. Haque, C. C. Havener, N. Shimakura, and M. Kimura, Phys. Rev. A **51**, 3685 (1995).
[42] J. H. Newman, J. D. Cogan, D. L. Ziegler, D. E. Nitz, R. D. Rundel, K. A. Smith, and R. F. Stebbings, Phys. Rev. A **25**, 2976 (1982).
[43] Y. Wu, Y. Y. Qi, S. Y. Zou, J. G. Wang, Y. Li, R. J. Buenker, and P. C. Stancil, Phys. Rev. A **79**, 062711 (2009); Y. Wu, Y. Y. Qi, J. Yan, J. G. Wang, Y. Li, R. J. Buenker, D. Kato, and P. S. Krstić, *ibid.* **80**, 022715 (2009); Y. Wu, J. G. Wang, P. S. Krstić, and R. K. Janev, J. Phys. B **43**, 201003 (2010).
[44] R. K. Janev, D. S. Belic, and B. H. Bransden, Phys. Rev. A **28**, 1293 (1983).
[45] V. A. Abramov, F. F. Baryshnikov, and V. S. Lisitsa, JETP Lett. **27**, 464 (1978).
[46] R. Ali, P. A. Neill, P. Beiersdorfer, C. L. Harris, D. R. Schultz, and P. C. Stancil, Astrophys. J. Lett. **716**, L95 (2010).